

Dynamics of Few Co-rotating Vortices in Bose-Einstein Condensates

R. Navarro¹, R. Carretero-González¹, P.J. Torres², P.G. Kevrekidis³,

D.J. Frantzeskakis⁴, M.W. Ray⁵, E. Altuntas⁵, and D.S. Hall⁵

¹*Nonlinear Dynamical Systems Group, Computational Science Research Center,
and Department of Mathematics and Statistics, San Diego State University, San Diego, CA 92182-7720, USA*

²*Departamento de Matemática Aplicada, Universidad de Granada, 18071 Granada, Spain*

³*Department of Mathematics and Statistics, University of Massachusetts, Amherst MA 01003-4515, USA*

⁴*Department of Physics, University of Athens, Panepistimiopolis, Zografos, Athens 157 84, Greece*

⁵*Department of Physics, Amherst College, Amherst, Massachusetts, 01002-5000 USA*

We study the dynamics of small vortex clusters with few (2–4) co-rotating vortices in Bose-Einstein condensates by means of experiments, numerical computations, and theoretical analysis. All of these approaches corroborate the counter-intuitive presence of a dynamical instability of symmetric vortex configurations. The instability arises as a pitchfork bifurcation at sufficiently large values of the angular momentum that induces the emergence and stabilization of *asymmetric* rotating vortex configurations. The latter are quantified in the theoretical model and observed in the experiments. The dynamics is explored both for the integrable two-vortex system, where a reduction of the phase space of the system provides valuable insight, as well as for the non-integrable three- (or more) vortex case, which additionally admits the possibility of chaotic trajectories.

Introduction. The realm of atomic Bose-Einstein condensates (BECs) [1] has offered a pristine setting for studies on the dynamics of few-vortex clusters [2]. Most investigations, however, have focused on either a single vortex or large scale vortex lattices [3–6]. Recently, theoretical investigations on the study of clusters of 2–4 vortices [7–15], have appeared, chiefly motivated by the experimental realizations of such states [16–19]. This focus has been heretofore centered on the fundamental building block of the vortex dipole, i.e., a pair of counter-circulating vortices.

Our aim in the present work, in contrast, is to explore the dynamics of small vortex clusters of 2–4 vortices that belong to the co-rotating (same charge) variety. The original work of Ref. [2] and subsequent efforts [20] have already paved the way for an understanding of symmetric few-vortex configurations rotating as a rigid body, and their three-dimensional generalizations, i.e., U- and S-shaped vortices, as well as vortex rings [21]. In this context, our work presents a rather unexpected twist: we have found that, under suitable conditions, the usual symmetric, co-rotating vortex configurations (centered line, triangle, and square) become *dynamically unstable*. More specifically, these states become subject to symmetry breaking, pitchfork bifurcations that lead to the spontaneous emergence of *stable asymmetric rotating vortex clusters*.

We present our analysis of these features in the integrable (at the reduced particle level) setting of a co-rotating vortex pair, and illustrate their generality by further considering a rigidly rotating vortex triplet and quadruplet. In the first case, we devise a theoretical formulation that not only explores the instability and manifests its growth rate, but also enables a visualization of a two-dimensional reduced phase space of the system in which the pitchfork bifurcation becomes transparent.

In the latter cases, we suitably parametrize the system, exploring the different regimes of symmetric and asymmetric periodic orbits. Our theoretical analysis treats vortices as classical particles, with dynamics governed by ordinary differential equations (ODEs). This reduction of the original vortex cluster system allows for the analytical characterization, numerical observation and experimental confirmation of the symmetry breaking phenomena.

Theoretical Analysis. As illustrated in Refs. [15, 19], and justified by means of a variational approximation [22], vortex dynamics governed by the two-dimensional mean-field Gross-Pitaevskii equation,

$$i\partial_t\psi = -\frac{1}{2}\Delta\psi + \frac{1}{2}\Omega^2(x^2 + y^2)\psi + |\psi|^2\psi, \quad (1)$$

can be reduced to a system of ODEs for the vortex positions. In the original partial differential equation (PDE) model (1), the time is measured in units of ω_z^{-1} , while the positions are measured in units of harmonic oscillator length along the z -direction and $\Omega = \omega_x/\omega_z = \omega_y/\omega_z$, with ω_j being the harmonic trap frequency along the j -direction (see, e.g., Ref. [4]). This ODE reduction is the starting point for our analysis in the co-rotating case.

The dynamics of vortex m at position (x_m, y_m) arises from two contributions: (i) a position-dependent vortex precession about the trap center with frequency $S_m \omega_{\text{pr}}$, and (ii) a vortex-vortex interaction with vortex n that induces a velocity perpendicular to their line of sight of magnitude $S_n \omega_{\text{vort}}/\rho_{mn}^2$, where ρ_{mn} is the distance between vortices m and n , S_m and S_n are their respective charges, and ω_{vort} is a dimensionless constant; see Ref. [15, 19]. The equations governing the dynamics of N interacting vortices embedded in a condensate are there-

fore

$$\begin{aligned}\dot{x}_m &= -S_m \omega_{\text{pr}} y_m - \frac{\omega_{\text{vort}}}{2} \sum_{n \neq m} S_n \frac{y_m - y_n}{\rho_{mn}^2}, \\ \dot{y}_m &= S_m \omega_{\text{pr}} x_m + \frac{\omega_{\text{vort}}}{2} \sum_{n \neq m} S_n \frac{x_m - x_n}{\rho_{mn}^2}.\end{aligned}\quad (2)$$

The precession about the trap center can be approximated by $\omega_{\text{pr}} = \omega_{\text{pr}}^0 / (1 - r^2/R_{\text{TF}}^2)$, where the frequency at the trap center is $\omega_{\text{pr}}^0 = \ln(A\frac{\mu}{\Omega})/R_{\text{TF}}^2$, μ is the chemical potential, $R_{\text{TF}} = \sqrt{2\mu}/\Omega$ is the Thomas-Fermi (TF) radius, and A is a numerical constant [3, 15, 19]. To describe better the actual vortex dynamics in the trap, the constant ω_{vort} in Eqs. (2) may be adjusted to account for the screening of vortex interactions due to the background density modulation [23].

We now focus on the case of two identical vortices of unit charge $S_1 = S_2 = 1$. We proceed to adimensionalize Eqs. (2) by scaling (x, y) by R_{TF} and time by $1/\omega_{\text{pr}}^0$, and use polar coordinates $(x_n, y_n) = (r_n \cos(\theta_n), r_n \sin(\theta_n))$. We then seek symmetric stationary states $r_1 = r_2 = r_*$ and $\theta_1 - \theta_2 = \pi$, and find the following frequency of the co-rotating vortices:

$$\omega_{\text{orb}} = \dot{\theta}_1 = \dot{\theta}_2 = \frac{c}{2r_*^2} + \frac{1}{1 - r_*^2}, \quad (3)$$

where $c = \frac{1}{2}(\omega_{\text{vort}}/\omega_{\text{pr}}^0)$ yields a measure of the relative strength of vortex interaction and spatial inhomogeneity. The comparison of the orbital frequency between the ODE and the PDE models is given in Fig. 1a. Given the co-rotating nature of this state, consideration of $\delta_{mn} = \theta_m - \theta_n$ renders this state a stationary one; linearizing around it using $r_m = r_* + R_m$ and $\delta_{mn} = \pi + \delta_m$ yields the following equations of motion for the perturbations about the symmetric equilibrium:

$$\ddot{R}_m = -\frac{\omega_{\text{ep}}^2}{2} (R_n - R_m), \quad \ddot{\delta}_m = -\frac{\omega_{\text{ep}}^2}{2} (\delta_m - \delta_n),$$

with $\omega_{\text{ep}}^2 = \frac{c^2}{2r_*^4} - \frac{2c}{(1-r_*^2)^2}$. It is then straightforward to observe that this squared epitrochoidal (motion of a point in a circle that is rotating about another circle) relative precession frequency of the two vortex positions and phases *changes sign* at $r_{\text{cr}}^2 = \sqrt{c}/(\sqrt{c} + 2)$. This signals our first fundamental result, namely the *destabilization* of the symmetric 2-co-rotating vortex state for sufficiently large symmetric distances of the vortices from the trap center. A comparison of the ODE and PDE models for the orbital and epitrochoidal precession frequencies for these two cases is given in Fig. 1a-b.

The dynamical instability of symmetric states suggests the potential existence of additional, asymmetric, ones. Seeking states with $\delta_{mn} = \pi$ and $r_1^* \neq r_2^*$ yields

$$-r_1^* r_2^* (r_1^* + r_2^*)^2 + c(1 - r_1^{*2})(1 - r_2^{*2}) = 0,$$

which will be the condition defining our radially *asymmetric* co-rotating solutions. The mirror symmetry of the 2-vortex system predisposes towards the pitchfork, symmetry breaking nature of the relevant bifurcation, a feature verified by the diagram of Fig. 1c. This diagram is given for the angle $\phi = \tan^{-1} r_2/r_1$ as a function of the angular momentum $L_0 = r_1^2 + r_2^2$, which is a conserved quantity for our system. It is interesting to note that if the single dimensionless parameter of the system is small ($c < 3$), then the critical value L_{cr} for L_0 —at which the bifurcation from symmetric to asymmetric periodic orbits occurs— is supercritical, while if c is sufficiently large ($c > 3$), it becomes subcritical [28] (not shown).

To elucidate the pitchfork nature of the bifurcation, we develop a phase plane representation for all 2-vortex configurations. The integrability of the reduced 2-particle description can be understood on the basis of the fact that this 4-dimensional system has two integrals of motion, namely the angular momentum L_0 , defined above, and the Hamiltonian H , which can be written in polar coordinates as

$$H = \frac{1}{2} \ln [(1 - r_1^2)(1 - r_2^2)] - \frac{c}{2} \ln [r_1^2 + r_2^2 - D],$$

where $D \equiv 2r_1 r_2 \cos(\delta)$ and $\delta = \theta_2 - \theta_1$. Using L_0 and the angle ϕ to express r_1 and r_2 , one can rewrite the Hamiltonian as a function of (ϕ, δ) having thus effectively reduced the 4-dimensional system into a 2-dimensional one. Thus, for different values of L_0 , we can represent the orbits in the effective phase plane of (ϕ, δ) in which the different orbits correspond to iso-energetic $H(\phi, \delta) = \text{const.}$ contours. This is done in Fig. 2 for values that are both below and above than the critical value of L_0 at fixed c . It can then be inferred that the symmetric fixed point with $(\phi, \delta) = (\pi/4, \pi)$ is stable in the former case, while it destabilizes in the latter case through the emergence of two additional asymmetric ($\phi \neq \pi/4$) states along the horizontal line $\delta = \pi$ of anti-diametric vortex states.

Remarkably, although the properties of the system dramatically change as we go from two vortices to three and four, the symmetry breaking bifurcation associated with the symmetric solutions persists. In particular, when $N > 2$, the persistence of the two conservation laws discussed above is not sufficient to ensure integrability of the system, and its absence is manifested in a dramatic form in the resulting 6 ($N = 3$) and 8 ($N = 4$) dimensional systems through the presence of chaotic orbits. Nevertheless, one can still theoretically analyze the highly symmetric co-rotating states of the system.

For $N = 3$, this state is an equilateral triangle such that $r_1 = r_2 = r_3 = r_*$ and $\delta_{i,i+1} = 2\pi/3$, with an orbital frequency predicted as $\omega_{\text{orb},3} = \frac{c}{r_*^2} + \frac{1}{1-r_*^2}$. In the co-rotating frame, the linear stability analysis around this rigidly rotating triangle can be performed giving rise to an epitrochoidal frequency $\omega_{\text{ep},3}^2 = \frac{c^2}{r_*^4} - \frac{2c}{(1-r_*^2)^2}$. In this case too, a critical radius exists $r_{\text{cr},3}^2 = \sqrt{c}/(\sqrt{c} + \sqrt{2})$,

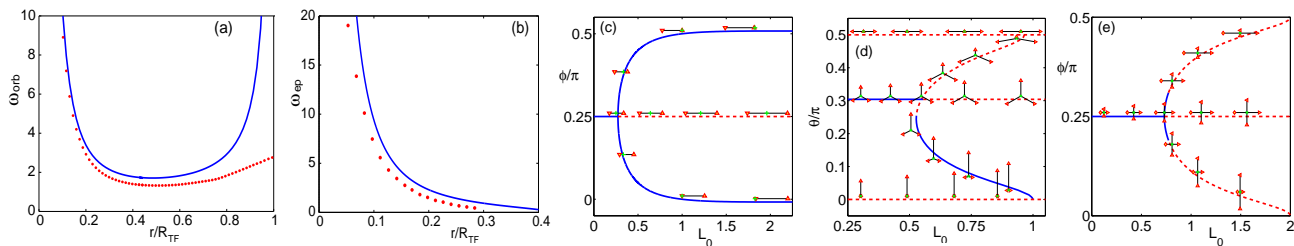


FIG. 1: (Color online) (a) Orbital and (b) epitrochoidal frequency as a function of the radial position from the trap's center for two vortices. Both frequency and radial position are in rescaled units. The solid line represents results from the ODE and the dotted line from the PDE. The vanishing of the latter signals the onset of instability. Here, $\Omega = 0.05$ and $\mu = 1$. Panel (c) depicts the quantity ϕ/π , which equals $1/4$ when $r_1 = r_2$, as a function of the square root of the angular momentum for $c = 0.1$. Panels (d) and (e) depict the corresponding phenomena for $N = 3$ and $N = 4$ vortices for $c = 0.1$. Panels (c), (d) and (e) include a few configurations along the main bifurcation branches ([blue] solid and [red] dashed lines corresponding, respectively, to stable and unstable configurations) depicting the relative position of the vortices (red triangles) with respect to the center of the condensate (green crosses).

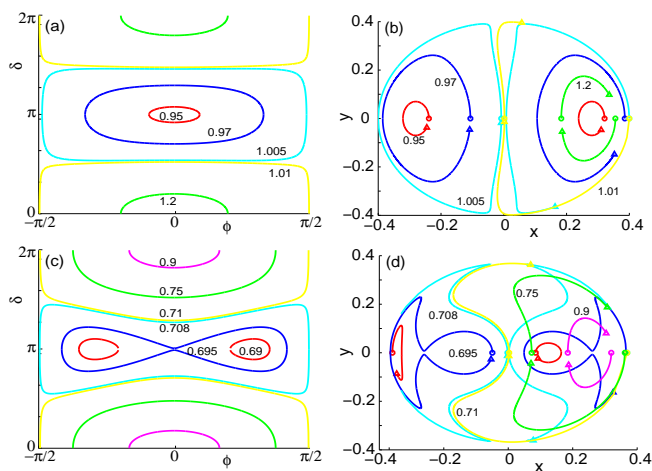


FIG. 2: (Color online) (a) Contours from the reduced Hamiltonian for vortices close to the center of the trap, i.e. $L_0 = 0.16$ below critical ($L_0 < L_{cr} = 0.273$), and (b) their corresponding orbits. Panels (c) and (d) depict, respectively, the same quantities but for vortices further out from the center for $L_0 = 0.36$ above critical ($L_0 > L_{cr} = 0.273$). The circles and triangles correspond, respectively, to the initial and final positions of the two vortices. Each color on the contour plot matches the corresponding orbit in the position diagram. Here, $c = 0.1$.

such that the symmetric state is destabilized and asymmetric orbits arise and are stable past this critical point as can be seen in Fig. 1d. The dynamical picture is considerably more complicated but the conservation of the angular momentum ensures that the dynamical evolution resides on the surface of a Bloch sphere. We thus define two angular variables $\tan \phi = r_2/r_1$ and $\cos \theta = r_3/\sqrt{L_0}$ and depict the associated pitchfork bifurcation in Fig. 1d for the subspace of solutions constrained to $r_1 = r_2$ and $\delta_{12} = \delta_{23}$. This bifurcation diagram describes a vortex configuration containing a stable symmetric rotating triangle before the bifurcation and stable asymmetric rotating triangles after the bifurcation. In addition to the equilibrium and near-equilibrium orbits, we observe

chaotic orbits arising both in a more localized form, exploring the vicinity of equilibrium orbits, and in a more extended one spanning all space (not shown).

While the general phenomena for $N = 4$ are already rather complex, some basic features can still be inferred and the symmetry breaking nature of the proposed instability persists —cf. Fig. 1e. Here, $\phi = \tan^{-1} r_3/r_1$, and we have constrained the vortices to be in a cross with right angles and $r_1 = r_3$ and $r_2 = r_4$. A general expression for the orbital frequency of the rigidly rotating state is $\omega_{orb,N} = \frac{(N-1)c}{2r_*^2} + \frac{1}{1-r_*^2}$, which is valid for any N . In the case of the square configuration with $r_i = r_*$ and $\delta_{i,i+1} = \pi/2$, there emerge two epitrochoidal vibrational motions with frequencies $\sqrt{-\lambda_1}$ and $\sqrt{-\lambda_2}$, where $\lambda_1 = \frac{3c}{(1-r_*^2)^2} - \frac{9c^2}{4r_*^4}$, and $\lambda_2 = \frac{4c}{(1-r_*^2)^2} - \frac{2c^2}{r_*^4}$. These, in turn, correspond to two critical points: one identical to the one given above for the $N = 3$ case, and one that is always higher, given by $r_{cr,4}^2 = \sqrt{3c}/(\sqrt{3c} + 2)$; hence, the same phenomenology persists.

Experimental Observations. We now briefly discuss experimental manifestations of the symmetry breaking events discussed above and of the emergence of asymmetric configurations.

The details of the experimental setup may be found elsewhere [17, 19]. We begin with a magnetically-trapped BEC of $N \sim 5-8 \times 10^5$ atoms in the $|F = 1, m_F = -1\rangle$ hyperfine level of ^{87}Rb . The radial and axial trap frequencies are $(\omega_r, \omega_z)/2\pi = (35.8, 101.2)$ Hz. Vortices are introduced through a process of elliptical magnetic trap distortion and rotation [24] during evaporation [25]. In terms of the trap frequencies along the major and minor axes of the distorted potential, ω_x and ω_y respectively, an ellipticity $\epsilon = (\omega_x^2 - \omega_y^2)/(\omega_x^2 + \omega_y^2) = 0.20$ and a rotation frequency of 8.5 Hz usually produces a co-rotating pair. Higher rotation frequencies are used to generate larger numbers of co-circulating vortices.

A partial-transfer (5%) imaging method [17] is employed to create a sequence of atomic density profiles,

as shown in Fig. 3a–d. The effect of the extractions is primarily to diminish the number of atoms in the condensate [14, 17]. Curiously, atomic losses have little effect on the calculated coupling parameter c , which scales only as $\log N$; thus c falls between 0.11 and 0.10 over the range $N = 0.3\text{--}0.8 \times 10^6$ atoms. For convenience, we take $c = 0.1$ in the following analysis.

We examine 52 experimental time series, each consisting of 8 snapshots spanning a total time of 240 to 480 ms. For each snapshot the center of the vortices and the radius of the BEC cloud are extracted using a least square fitting algorithm [see panels a)–d) in Fig. 3]. The vortex positions are then normalized to the BEC radius (i.e., TF units) and the angular momentum L_0 and Hamiltonian H were computed for each frame [see panels e)–h) in Fig. 3]. For each series, the averaged angular momentum \bar{L}_0 and Hamiltonian \bar{H} are computed (see horizontal dashed lines in the middle panels in Fig. 3). Using \bar{L}_0 we compare the experimental points representing each orbit in the (ϕ, δ) plane to the isocontour of H corresponding to \bar{H} , as shown in the right column of panels in Fig. 3, and find good agreement between the two.

The panels a)–d) in Fig. 3 depict a cohort of typical time series, together with their respective fits, that exemplify the different qualitative cases that we observed in the experiments. In particular, we find that the dynamics of the vortices depends on whether the average angular momentum is below or above the critical threshold $L_{\text{cr}} = 2r_{\text{cr}}^2$. This separates cases where asymmetric orbits are, respectively, non-existent and possible. The different qualitative cases that we observe, which are displayed in Fig. 3, may be grouped as follows:

- For $\bar{L}_0 < L_{\text{cr}}$ and relatively small \bar{H} , the experiment displays *symmetric* orbits. See rows a) and e) in Fig. 3.
- For $\bar{L}_0 > L_{\text{cr}}$ and moderate \bar{H} , the experiment displays (i) *symmetric* orbits where both vortices (in the co-rotating frame) are approximately on the *same* side of the cloud chasing each other on the same path [see rows b) and f) in Fig. 3] or (ii) *asymmetric* orbits [see rows c) and g) in Fig. 3]. The choice between these two orbits is determined by the initial conditions. Initial conditions inside the area delimited by the separatrix (red double-loop curve in the right panels of Figs. 3.f and Figs. 3.g) emanating from the saddle point $(\phi, \delta) = (\pi/4, \pi)$ give rise to asymmetric orbits.
- For $\bar{L}_0 > L_{\text{cr}}$ and large \bar{H} , the experiment displays orbits in which one vortex remains close to the center while the other orbits around it close to the periphery of the cloud. See rows d) and h) in Fig. 3.

As is clear from these examples and the remaining 48 data sets that we studied (see supplemental material), asymmetric orbits are only found when $\bar{L}_0 > L_{\text{cr}}$ and when the vortex orbits fall inside the asymmetric minima regions of the Hamiltonian picture in the (ϕ, δ) plane. Asymmetric solutions absent in all of the cases for which $\bar{L}_0 < L_{\text{cr}}$. These results are in good agreement with

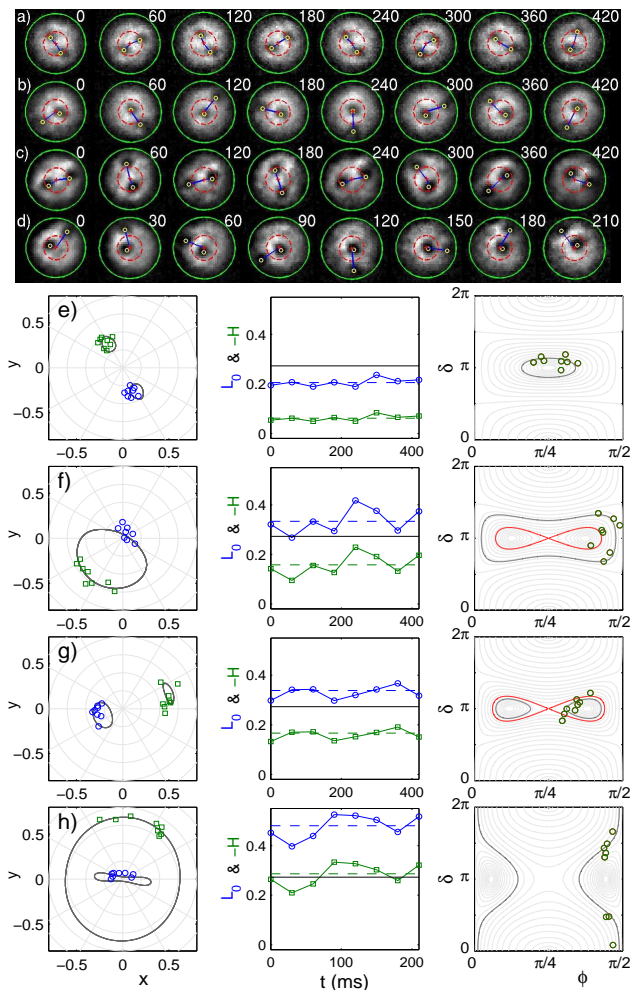


FIG. 3: (Color online) a)–d) Typical experimental series for the dynamics of two co-rotating vortices (time indicated in ms). The large (green) circles and the red crosses represent, respectively, the fitted TF radius and center of the cloud while the small (yellow) dots depict the fitted vortex centers. The (red) dashed circles represent the critical radius, r_{cr} , above which symmetric orbits become unstable. e)–h) Manifestation of the pitchfork bifurcation for the experimental series depicted in panels a)–d) which correspond to $c = 0.1$. Left column: experimental vortex positions and their corresponding orbit from the reduced ODE model (solid line), in TF units in the co-rotating frame. Middle column: corresponding L_0 (blue circles) and $-H$ (green squares) and their averages (horizontal dashed lines) as well as the critical value for L_0 (solid horizontal line). Right column: corresponding orbits in the (ϕ, δ) plane along with isocontours for constant H (highlighted in dark gray is the isocontour corresponding to the average H and in red is the separatrix delimiting the area containing asymmetric orbits).

the theoretical prediction of the pitchfork bifurcation depicted in Fig. 1c.

To extend our considerations, we briefly present a comparison between experiment and theory for $N = 3$ and $N = 4$ vortices. The main phenomenology is depicted

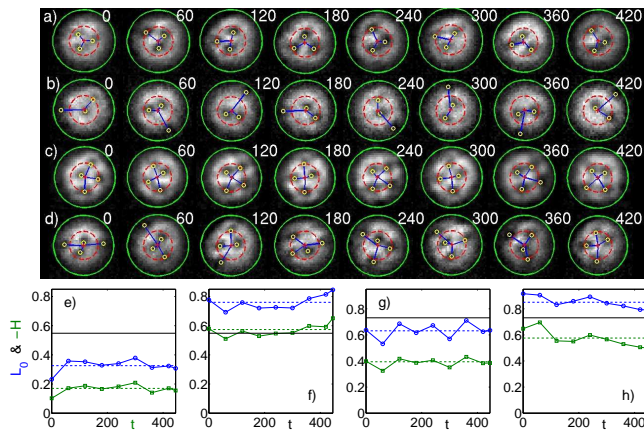


FIG. 4: (Color online) Experimental series for trios [a) and b)] and quartets [c) and d)] below [a) and c)] and above [b) and d)] the critical threshold. e)–h) Corresponding time series for L_0 and $-H$. Same notation and units as in Fig. 3.

using two examples for each case in Fig. 4. Panels a) and b) correspond to the $N = 3$ vortex case below and above the pitchfork bifurcation [see panel e) and f)]. Panels c) and d) depict the equivalent scenario for $N = 4$ vortices. As the figure illustrates, and is observed in all of the cases that we studied (17 data sets for $N = 3$ and 5 data sets for $N = 4$; not shown), the main phenomenology for $N = 3$ and $N = 4$ persists in that all configurations with $\bar{L}_0 > L_{cr}$ are not symmetric and symmetric configurations, or epitrochoidal oscillations about them, are only present when $\bar{L}_0 < L_{cr}$.

Conclusions. We have revisited the theme of co-rotating few vortex clusters in atomic Bose-Einstein condensates. By a combination of theoretical analysis, numerical computation and experimental observation, we have illustrated a strong manifestation of symmetry breaking through a pitchfork bifurcation, which led to the destabilization of symmetric solidly rotating configurations and gave rise to the emergence of *stable* co-rotating but *asymmetric* vortex configurations. We showed that this analysis is fruitful not only for the integrable (at the reduced particle level) two-vortex setting, where a suitable parametrization of the phase space was provided, but also for the non-integrable cases of $N = 3$ and $N = 4$ vortices where chaotic orbits exist.

Naturally, it would be interesting to provide a more global characterization of the dynamics of the three-body problem, which is perhaps the most analytically tractable and interesting case due to its potential for chaos. Another expansion of the present considerations involves their generalization to higher dimensions. In this case, it would be interesting to see, upon gradual decrease of the trapping frequency in the third dimension, whether the symmetry-breaking phenomena persist for line vortices and vortex rings. These aspects are presently under study and results will be reported elsewhere.

exp#	\bar{L}_0	\bar{H}	exp#	\bar{L}_0	\bar{H}
a)	0.098	0.0533	aa)	0.219	-0.061
b)	0.117	0.0188	bb)	0.220	-0.069
c)	0.118	0.0175	cc)	0.221	-0.033
d)	0.125	0.0282	dd)	0.224	-0.058
e)	0.131	0.0049	ee)	0.247	-0.088
f)	0.134	0.0062	ff)	0.254	-0.085
g)	0.146	-0.0056	gg)	0.257	-0.078
h)	0.147	-0.0099	hh)	0.257	-0.087
i)	0.153	-0.0125	ii)	0.282	-0.111
j)	0.157	-0.0216	jj)	0.282	-0.105
k)	0.157	-0.0177	kk)	0.300	-0.075
l)	0.164	-0.0162	ll)	0.306	-0.137
m)	0.167	-0.0294	mm)	0.307	-0.135
n)	0.167	-0.0230	nn)	0.333	-0.157
o)	0.169	-0.0215	oo)	0.338	-0.166
p)	0.172	-0.0273	pp)	0.366	-0.185
q)	0.179	-0.0378	qq)	0.373	-0.196
r)	0.184	-0.0404	rr)	0.438	-0.241
s)	0.187	-0.0429	ss)	0.480	-0.286
t)	0.193	-0.0392	tt)	0.519	-0.335
u)	0.194	-0.0517	uu)	0.558	-0.372
v)	0.194	-0.0509	vv)	0.619	-0.382
w)	0.205	-0.0617	ww)	0.655	-0.471
x)	0.208	-0.0634	xx)	0.664	-0.489
y)	0.213	-0.0488	yy)	0.690	-0.606
z)	0.213	-0.0697	zz)	0.751	-0.478

TABLE I: Averaged angular momentum \bar{L}_0 and averaged Hamiltonian \bar{H} for all the experimental series containing two co-rotating vortices. The critical angular momentum for the experimental setup is $L_{cr} = 0.2731$.

Acknowledgments: Support from NSF PHY-0855475 (D.S.H.), NSF DMS-0806762 and CMMI-1000337, and Alexander von Humboldt Foundation (P.G.K.), and NSF DMS-0806762 (R.C.G.), and discussions with T.K. Langin are kindly acknowledged.

SUPPLEMENTAL MATERIAL:

Here we present the results that we obtained for the 52 experimental series containing two co-rotating (same charge) vortices. The experiments are ordered by the average angular momentum \bar{L}_0 , which is computed from the fitted centers and cloud diameter. The average is then computed by averaging over the eight experimental snapshots for each series. Table I lists the average angular momentum and average Hamiltonian for all the experimental series containing two co-rotating vortices. The corresponding snapshots for all the series are shown in Fig. 5 using the same ordering as given in Table I. Finally, Fig. 6 depicts the analysis for each individual series by presenting the orbits in the co-rotating frame (respective

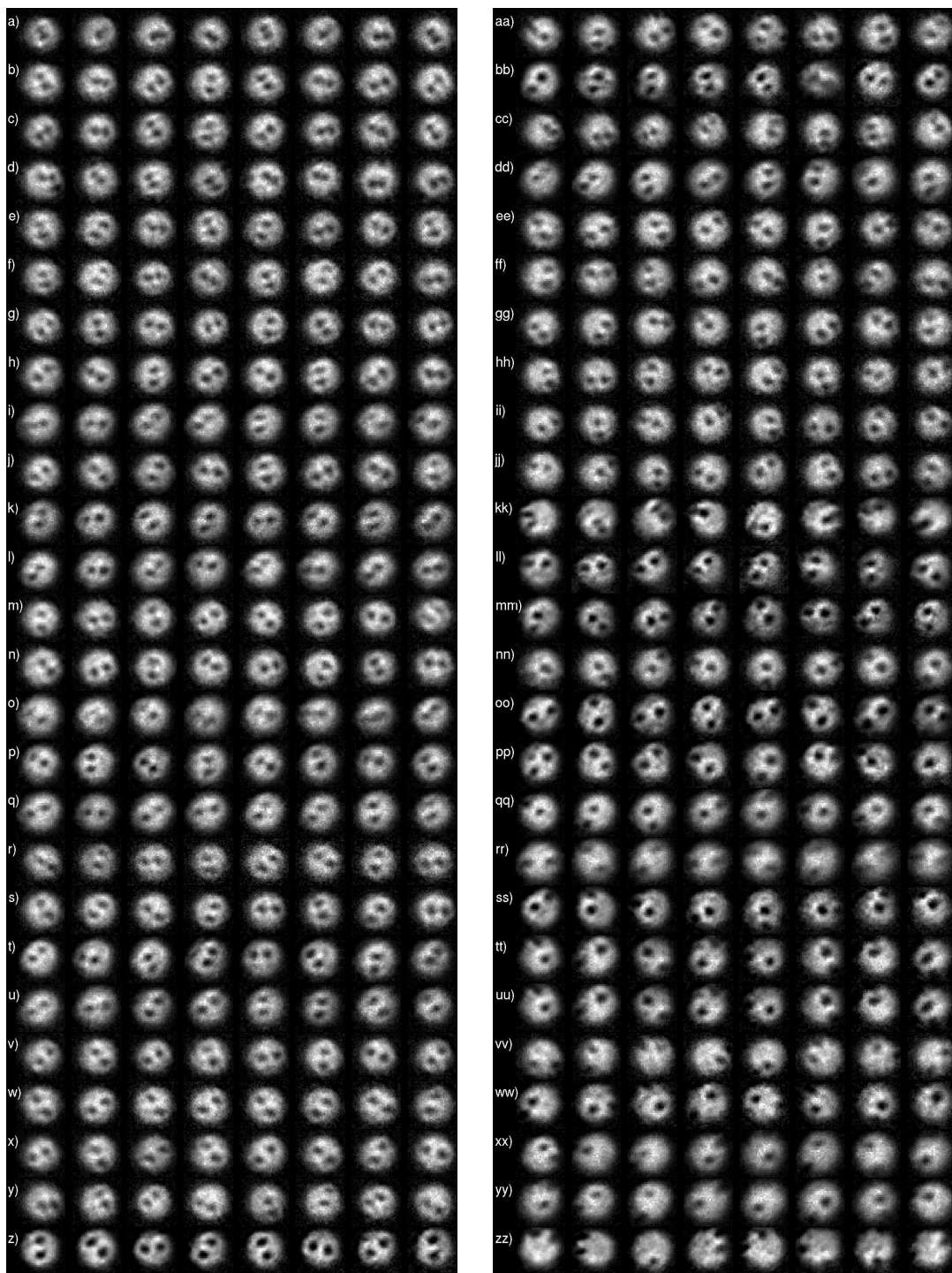


FIG. 5: Experimental time series corresponding to the 52 experiments containing two co-rotating vortices. The snapshots were taken at regular times for a total time spanning 240 ms or 480 ms (for individual times for each snapshot refer to the corresponding middle column in Fig. 6). The experiments are ordered according to average angular momentum as listed in Table I. For ease of presentation, all the images have been centered and rescaled so that they occupy approximately the same visual area.

left columns), the times series for the angular momentum and Hamiltonian (respective middle columns), and the orbits in the reduced (ϕ, δ) plane (respective right columns).

As observed in Fig. 6, the experimental orbits in the co-rotating frame (respective left columns) match well the theoretical orbits from our model (see gray orbit for all of the experimental runs. Significantly also, all ex-

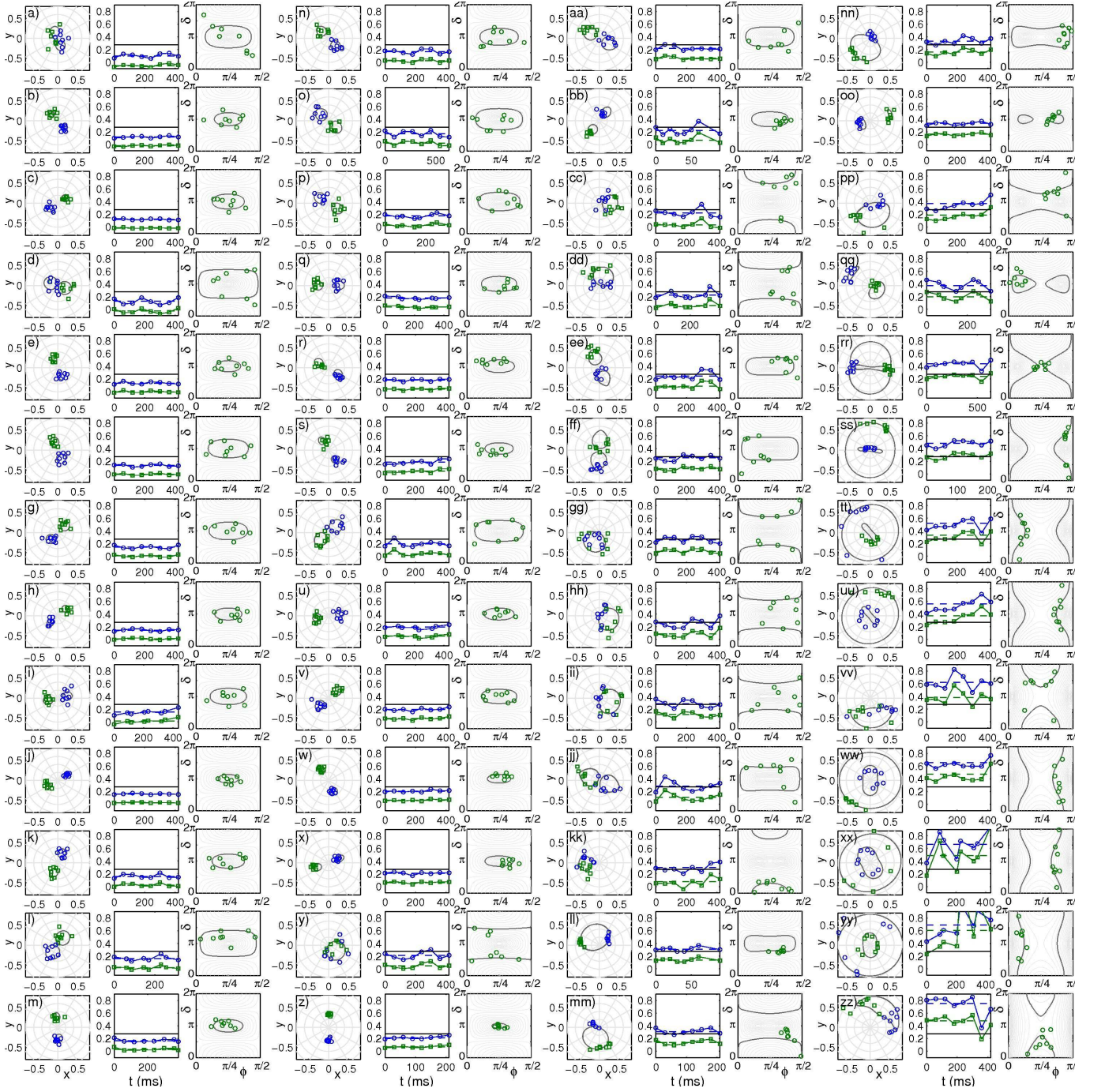


FIG. 6: (Color online) Analysis for experimental series depicted in Fig. 5. For each series the respective columns represent: (i) The left column depicts the vortex orbits (green squares and blue circles), and their corresponding orbit from the reduced ODE model (gray solid line), in TF units in the co-rotating frame. (ii) The middle column depicts the time series for the angular momentum L_0 (blue circles) and negative Hamiltonian $-H$ (green squares) and their respective averages (horizontal dashed lines) as well as the critical value for L_0 (solid horizontal line). (iii) The right column depicts the orbits in the (ϕ, δ) plane along with the isocontours for constant H (highlighted is the isocontour corresponding to the average H).

perimental orbits in the reduced (ϕ, δ) plane (respective right columns) match well the theoretical orbits corresponding to the isocontour of constant H equal to the average H from the experiment —with the exception of the experiment #rr which we discuss below. In most of

the experimental series both the angular momentum and the Hamiltonian are approximately conserved, buttressing the validity of our dynamical reduction.

To further bolster the case for the validity of our reduced dynamics we now concentrate on the main result

of our manuscript. The reduced model predicts that, as the angular momentum is increased, the co-rotating symmetric configuration loses stability in a pitchfork, symmetry-breaking bifurcation. At the bifurcation point a pair of stable, asymmetric co-rotating configurations emerge. Here, the bifurcation point is predicted to occur at $L_{\text{cr}} = 2r_{\text{cr}}^2$ where the square of the critical radius is $r_{\text{cr}}^2 = \sqrt{c}/(\sqrt{c} + 2)$ in units of the Thomas-Fermi radius. In our experiment, the value of c , the ratio between the rotation induced by vortex-vortex interactions and the rotation induced by the precession of vortices due to the inhomogeneity of the cloud's background produced by the external magnetic trap, is $c \approx 0.1$. This gives a value for the critical angular momentum in our experiments of $L_{\text{cr}} = 0.2731$. Therefore, corroboration of our analytical prediction about the pitchfork bifurcation would imply that (i) for all the experimental series with an average angular momentum below critical ($\bar{L}_0 < L_{\text{cr}}$) there should be no co-rotating asymmetric orbits, and (ii) if an asymmetric co-rotating orbit is observed its corresponding angular momentum should be above the critical threshold. The critical threshold for the angular momentum lies between experiments#hh and ii.

It should be noted at this stage that an angular momentum above critical does not imply an asymmetric co-rotating orbit. For example orbits with high angular momentum (see experiments#ss-zz) might correspond to (i) orbits where vortices seem decoupled and one vortex remains close to the trap center while the other orbits around close to the periphery of the cloud (see experiments#ss, tt, uu, ww, xx, yy), or (ii) the two vortices belong to the same path that has them on the same side of the cloud (see experiments#vv and zz). The type of resulting orbit is heavily dependent on the initial conditions. In fact, in the (ϕ, δ) plane, the area of the set of initial conditions that leads to co-rotating asymmetric orbits (or slight perturbations thereof) is rather small and therefore asymmetric co-rotating instances are less common. Nonetheless, we were able to identify two orbits as being asymmetric (i.e., epitrochoidal perturbations of the asymmetric orbit) in experiments#oo and qq. In fact experiment#oo is featured in panels c) and g) in Fig. 3 of the manuscript. It is reassuring that the angular momenta corresponding to the experimental asymmetric cases is clearly above critical supporting our dynamical reduction and the pitchfork bifurcation picture that it unveiled.

It is important to note that one of the 52 experimental series did not match our theoretical expectations. This case is experiment#rr. As it is clear from the right panel of Fig. 6.rr, the experimental orbit lies close to the point $(\phi, \delta) = (\pi/4, \pi)$ indicating an almost perfect *symmetric* orbit as observed in the left panel of Fig. 6.rr. However, this case has an average angular momentum of $\bar{L}_0 = 0.438$, well above the critical threshold $L_{\text{cr}} = 0.2731$. The reduced dynamics description predicts

that this orbit should be unstable, lying as it does close to an unstable saddle. It is not clear how this symmetric orbit can exist in this supposedly unstable region. It is possible, albeit unlikely, that this is an unstable orbit that has not had enough time for the instability to develop. A second, more plausible, explanation can be given if one carefully examines the experimental snapshots corresponding to this experiment depicted in Fig. 5.rr. It is evident that in this experimental series, the traces of the vortices are much more diffuse and blurry than in the other series. The vortex lines corresponding to the vortices in this series may not be straight or aligned with the trap axis but rather bent [26, 27]. This explains on one hand the blurriness of the vortex cores in the experimental snapshots and the unusual (with respect to our analytical dynamical reduction) dynamics that they display. This would further serve to illustrate the consequence of the true three-dimensional nature of the condensate that, in some instances, cannot be captured by our reduced *two-dimensional* description.

-
- [1] C.J. Pethick and H. Smith, Bose-Einstein Condensation in Dilute Gases, Cambridge University Press (2002); L. Pitaevskii and S. Stringari, Bose-Einstein Condensation, Oxford University Press, New York (2003).
 - [2] Y. Castin and R. Dum, Eur. Phys. J. D, **7**, (1999) 399.
 - [3] A.L. Fetter and A.A. Svidzinsky, J. Phys.: Condens. Matter, **13** (2001) R135.
 - [4] P.G. Kevrekidis, D.J. Frantzeskakis and R. Carretero-González, Emergent Nonlinear Phenomena in Bose-Einstein Condensates, Springer-Verlag, Berlin (2008).
 - [5] A.L. Fetter, Rev. Mod. Phys., **81** (2009) 647.
 - [6] P.K. Newton and G. Chamoun, SIAM Review **51**, 501 (2009).
 - [7] L.-C. Crasovan, *et al.*, Phys. Rev. E, **66** (2002) 036612.
 - [8] L.-C. Crasovan, *et al.*, Phys. Rev. A, **68** (2003) 063609.
 - [9] Q. Zhou and H. Zhai, Phys. Rev. A, **70** (2004) 043619.
 - [10] M. Möttönen, *et al.*, Phys. Rev. A, **71** (2005) 033626.
 - [11] V. Pietilä, *et al.*, Phys. Rev. A, **74** (2006) 023603.
 - [12] W. Li, *et al.*, Phys. Rev. A, **77** (2008) 053610.
 - [13] S. Middelkamp, *et al.*, Phys. Rev. A, **82** (2010) 013646.
 - [14] P. Kuopanportti, *et al.*, Phys. Rev. A, **83** (2011) 011603.
 - [15] P.J. Torres, *et al.*, Phys. Lett. A **375**, 3044 (2011).
 - [16] T.W. Neely, *et al.*, Phys. Rev. Lett. **104** (2010) 160401.
 - [17] D.V. Freilich, *et al.*, Science, **329** (2010) 1182.
 - [18] J.A. Seman, *et al.*, Phys. Rev. A, **82** (2010) 033616.
 - [19] S. Middelkamp, *et al.*, Phys. Rev. A **84**, 011605(R) (2011).
 - [20] A. Aftalion and I. Danaila. Phys. Rev. A, **68** (2003) 023603; *ibid.* Phys. Rev. A, **69** (2004) 033608; I. Danaila. Phys. Rev. A, **72** (2005) 013605.
 - [21] S. Komineas, Eur. Phys. J.-Sp. Top. **147**, 133 (2007).
 - [22] D.E. Pelinovsky and P.G. Kevrekidis, Nonlinearity **24**, 1271 (2011).
 - [23] S. McEndoo and Th. Bush, Phys. Rev. A, **79** (2009) 053616.
 - [24] E. Hodby, *et al.*, Phys. Rev. Lett. **88** (2001) 010405.
 - [25] K.W. Madison, *et al.*, Phys. Rev. Lett. **84** (2000) 806.

- [26] A. Aftalion and I. Danaïla, Phys. Rev. A **68** (2003) 023603.
- [27] S. Komineas, N. R. Cooper and N. Papanicolaou, Phys. Rev. A **72** (2005) 053624.
- [28] It should be noted here, however, that the latter bifurcation is merely of mathematical interest, as for typical values of the physical parameters, the supercritical scenario is the one which is realized.